

# Taskology: Utilizing Task Relations at Scale

Yao Lu<sup>1,2</sup>, Sören Pirk<sup>1,2</sup>, Jan Dlabal<sup>2</sup>, Anthony Brohan<sup>1,2</sup>, Ankita Pasad<sup>3,\*</sup>, Zhao Chen<sup>4</sup>,  
Vincent Casser<sup>4</sup>, Anelia Angelova<sup>1,2</sup>, Ariel Gordon<sup>1,2</sup>

<sup>1</sup>Robotics at Google <sup>2</sup>Google Research <sup>3</sup>Toyota Technological Institute at Chicago <sup>4</sup>Waymo LLC

\*

## Abstract

*It has been recognized that the joint training of computer vision tasks with shared network components enables higher performance for each individual task. Training tasks together allows learning the inherent relationships among them; however, this requires large sets of labeled data. Instead, we argue that utilizing the known relationships between tasks explicitly allows improving their performance with less labeled data. To this end, we aim to establish and explore a novel approach for the collective training of computer vision tasks. In particular, we focus on utilizing the inherent relations of tasks by employing consistency constraints derived from physics, geometry, and logic. We show that collections of models can be trained without shared components, interacting only through the consistency constraints as supervision (peer-supervision). The consistency constraints enforce the structural priors between tasks, which enables their mutually consistent training, and – in turn – leads to overall higher performance. Treating individual tasks as modules, agnostic to their implementation, reduces the engineering overhead to collectively train many tasks to a minimum. Furthermore, the collective training can be distributed among multiple compute nodes, which further facilitates training at scale. We demonstrate our framework on subsets of the following collection of tasks: depth and normal prediction, semantic segmentation, 3D motion estimation, and object tracking and detection in point clouds.*

## 1. Introduction

Many tasks in computer vision, such as depth and surface normal estimation, flow prediction, pose estimation, semantic segmentation, or classification, aim to achieve an understanding of scenes along with their dynamics. While solving for each of these tasks may require specialized methods, most tasks are inherently connected by the underlying physics governing real scenes. A considerable amount

of research aims to reveal the relationships between tasks (e.g. [86, 9, 20, 82, 18]), but only a few methods explicitly utilize these priors. To the contrary, many approaches rely on the often unparalleled performance of deep neural networks to learn mappings between tasks [81]. However, training individual tasks in isolation does not leverage their relationships and also leads to inconsistencies when building perception frameworks of independently trained tasks.

Multi-task learning targets this problem by training multiple tasks jointly. Common to many approaches is a shared feature-extractor component with multiple “heads” that perform separate tasks [20, 82, 18]. Training multiple tasks together increases the coherency between tasks and – in some setups – also enables their self-supervision [86, 9]. However, the joint training also has a few disadvantages. For one, a single model for multiple tasks is difficult to design, maintain and improve, as any change in the training data, the losses, or the hyperparameters associated with one of the tasks also affects all others. Second, it can become intractable to process a single model – built to perform multiple tasks – on a single compute node. Third, while distributed training addresses these problems through processing models based on model- or data parallelism, almost all distributed training schemes follow rather strict synchronization schemes for performing gradient updates.

In this paper we introduce a novel approach for distributed collective-training that explicitly leverages the connections between multiple tasks based on consistency losses (Fig. 1). Consistency losses are designed for sets of tasks and are supposed to enforce their logical or geometric structure. For example, given the two tasks of predicting surface normals and depth from RGB images, the consistency loss between them can be the analytical relation that normals can be computed from the derivatives of a depth map. Explicitly enforcing consistency between tasks can improve their individual performance, while their collective training also establishes coherency between individual tasks and therefore a more sound visual understanding of the whole scene.

Moreover, using consistency losses to co-train tasks enables a modular design for training neural networks, which offers three major advantages: for one, we can train struc-

\*Work done while at Robotics at Google.

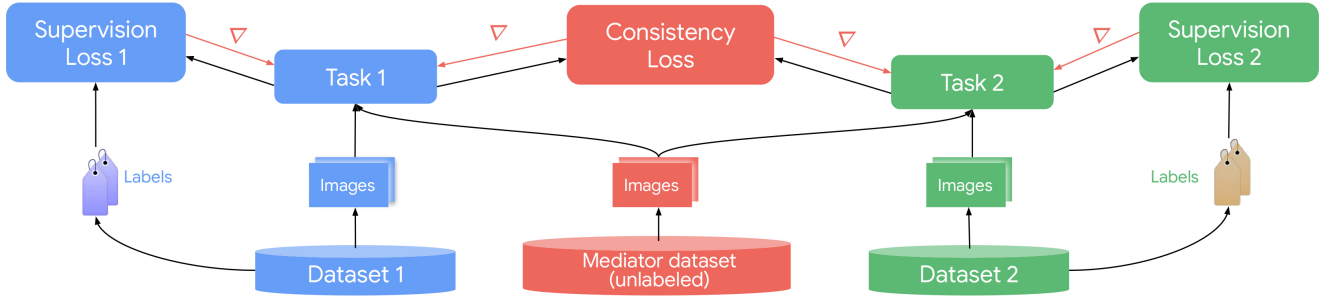


Figure 1. Illustration of our framework for the collective training of two tasks with a consistency loss. Each task is performed by a separate network, and trained on a mixture of its own dataset and an unlabeled *mediator* dataset. The consistency loss is only imposed for sampled from the mediator dataset.

turally different tasks with entirely separate networks that are better suited for each individual task. Second, we can design tasks as modules, which – similar to modular programming – allows combining them in a scalable manner; we argue that a multi-task system built from disjoint networks, where each one of them performs a separate task, is advantageous from a design, development, and maintainability point of view – each component can be replaced or improved separately from all others. Finally, we can train multiple complex models jointly and asynchronously on different compute nodes.

We show that a modular design enables massive parallelism. Each network can be processed on a separate machine, while their training is tied together through consistency losses. The communication between collectively trained networks – through their predictions – can be asynchronous. Our experiments show that networks for different tasks can be trained with stale predictions from their peers; we do not observe a decrease in performance for up to 20 minute old predictions. Unlike existing methods for distributed training [54] that mostly rely on data- or model parallelism to split training across multiple compute nodes, our framework separates training at task level; each model is trained independently and asynchronously from all other models, while all models are coherently trained together. This approach to distributed training allows us to train multiple tasks jointly, with the advantages introduced by multi-task training [85, 68], while it also facilitates training at scale with more relaxed latency requirements.

Finally, by introducing consistency losses, we exploit the existing knowledge of tasks and thereby combine the strengths of data- and model-based approaches in computer vision. In summary, the main contributions of this work are:

- we present a framework that enables a modular design for training neural networks by separating tasks into modules that can be combined and then trained collectively;

- we introduce task-level distributed training of neural networks, as opposed to model- or data level parallelism;
- we propose using consistency losses for coherently co-training multiple tasks that allows improving their overall performance;
- we analyze the trade-off between latency, accuracy, and training time for the collective training of multiple tasks;
- we show that collectively trained tasks supervise themselves, which reduces the need for labeled data.

## 2. Related Work

Exploiting the structure of – and between – tasks has a long tradition in computer science [74, 77] and computer vision [53]. It has been recognized that knowing about the structure of a task and how it is related to other tasks can be used as a powerful learning scheme [81, 7, 86, 9, 31]. In our work we are interested in making use of these relations more explicitly through the joint co-training of multiple tasks based on consistency losses. Therefore, our method is connected to related work on self- and unsupervised learning, multi-task learning, domain adaptation, and distributed training. While this spans a breadth of related work that we cannot conclusively discuss, we aim to provide an overview of approaches closest to ours with a focus on computer vision.

**Self-supervised Learning:** methods based on self-supervision aim to autonomously generate labels for training data based on exploiting the inherent structure of tasks and their relationships. As a prominent example, Doersch et al. [19] use unlabeled image collections to learn a representation for recognizing objects. Similarly, many other approaches use proxy or surrogate tasks to learn rich representations for visual data [60, 62, 84, 82, 61]. Self-supervised

learning is closely related to our approach as we aim to self-supervise a collection of tasks by establishing consistency losses between them. By designing the consistency losses we directly make use of the known relations between tasks and thereby shape the tasks space, which is similar to common self-supervised training schemes.

**Unsupervised Learning:** the goal of unsupervised techniques is to identify patterns in data to learn more compact representations [4]. A variety of methods exists to learn such representations through the means of auto-encoding [44], adversarial feature learning [21], clustering [5], or dimensionality reduction [28, 67]. Our approach is not – in general – unsupervised. While some tasks may be trained in an unsupervised manner through the consistency losses (e.g. depth and ego-motion), we rely on labeled-data for other tasks. Furthermore, our goal is not to learn a representation, but to facilitate the learning of individual tasks by exploiting their relationships.

**Multi-Task Learning:** training models for tasks so as to obtain multiple outputs for a given input, while jointly improving the performance of each individual tasks is the goal of multi-task learning [8, 85, 68]. Many approaches exist that extract features through a shared backbone and then train multiple heads for different objectives [20, 82]. These approaches are often restricted to tuning the loss function to balance contributions between different tasks [12, 43, 70]. Beyond that restriction, a major challenge many existing approaches face is the complexity of training multiple models, which extends to finding the correct hyperparameters and losses [20] to managing different datasets as well as to establishing lightweight compute and memory footprints [46]. A large body of work exists that focuses on the different aspects of multi-task learning. This spans as far as from learning visual features [66] or policies [73] based on simulated data, to learning unlabeled tasks [63], or – more generally – representations [76] with a focus on shared [59] or even recurrent features [6]. Our approach is closely related to previous work on multi-task learning; however, unlike the existing approaches our goal is not to learn specific tasks or to learn them through shared backbones. Instead, we propose a general and modular approach for jointly training different models through consistency losses.

**Domain Adaptation:** approaches for domain adaptation aim at learning a task from a source data distribution with the goal to perform well on a target data distribution. Methods for domain adaptation focus on regularized training [3], adapting embeddings [39] or kernels [48] through transformations, explicitly shifting distributions [80], or closed-form sub-space alignment [26]. A number of methods specifically focus on computer vision tasks, for example, by considering domain-related visual features [69] or by learning intermediate representations [33]. In this work we do not specifically target domain adaptation, however, we can

use our framework for transfer learning by co-training two models on the same task, but based on different sources of data, which is particularly useful if labels for one domain (e.g. simulation) are easier to obtain than for another (e.g. real).

**Computer Vision Tasks:** while our framework is not limited to any specific task domain or combination of tasks, in this work we focus on the collective training of computer vision models. To this end, we are interested in using established methods for learning depth [31, 24, 49, 86] also together with egomotion [86, 9], surface normals [83, 18, 37, 29, 64, 75], segmentation [71, 52, 42], optical flow [22, 40, 65, 13], object classification and detection [25, 36, 41], or point cloud tracking [35, 1]. While we do not aim to change the model architectures for any of these tasks, our goal is to improve their performance by designing consistency losses for subsets of these tasks and by jointly training them.

**Distributed Training:** due to the importance of training complex deep neural networks a number of methods study the distributed training of model architectures mostly with an emphasis on model [17, 27, 55, 57, 58] or data [79, 47, 78] parallelism; the recent survey of Mayer and Jacobsen [54] provides a thorough overview. While model parallelism aims at slicing a model so as to train its individual parts on multiple workers, data parallelism focuses on training the same model on disjoint sets of data to then combine the generated training signals. Both approaches implement distributed training by synchronizing based on the weights that result from the training procedure, which requires low latency between compute units as well as between training iterations.

Unlike these existing techniques, our framework implements distributed training at the level of tasks. We do not slice models or data, but instead train individual models independently and with their own data as if they are trained in isolation. However, we use consistency losses, to also jointly train the models, which allows us to obtain more coherent training signals with all the advantages of common multi-task learning setups. Finally, our framework is closely related to the concept of distillation [38] or online distillation [2], where one network is trained toward an objective with the goal to guide the training of another network. However, unlike them, we advance the concept of this variant of distributed training by explicitly leveraging the structure between tasks and by training multiple complex vision tasks simultaneously.

### 3. Method

Our main goal is to enable the distributed and collective training of individual network architectures for computer vision tasks that are inherently related. To train models collectively, we use existing model architectures for specific

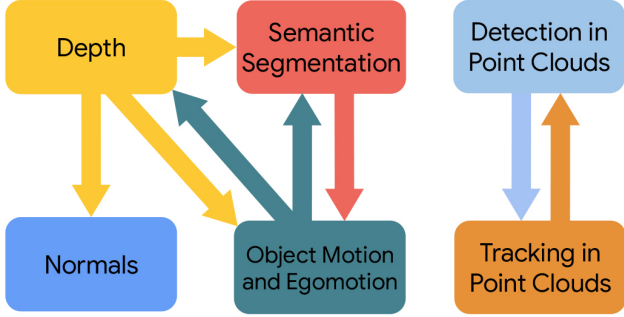


Figure 2. Task relations: arrows indicate which consistency losses we introduce to co-train different pairs of tasks.

tasks (e.g. such as for predicting depth or surface normals) and define a consistency loss between them. In this section we describe our framework, the co-training of two or multiple tasks, the motivation for consistency losses, as well as the distributed co-training of multiple models.

### 3.1. Task Consistency Constraints

We rely on the established knowledge in computer vision of tasks and their relationships to identify *consistency constraints*. Consistency constraints ensure the coherency between different tasks and are derived from laws of geometry and probability. Our goal is to leverage the consistency constraints to define *consistency losses* for task combinations. Any constraint that can be written as differentiable analytic expression can be used within our framework.

In particular, we aim to exploit consistency constraints relating the tasks of predicting depth, surface normals, egomotion, semantic segmentation, object motion, and object tracking with 2D and 3D sensor data (Fig. 2). For some tasks it is possible to directly formulate their relationship as an analytical differentiable expression – e.g. normals can be computed from the derivatives of depth values, other tasks are related in more intricate ways, e.g., depth, ego motion, segmentation, and optical flow [34, 9, 13]. In the following, we provide examples for consistency constraints utilized here:

**Geometric Consistency:** given a depth prediction module and a surface-normal prediction module, we can assert that the normals obtained from the spatial derivatives of the depth map are coherent with the predicted normals.

**3D Motion Consistency:** a dynamic scene can be decomposed into moving objects. Given a module that segments movable objects in a scene, in two consecutive frames, and another module that predicts rigid motion, we can assert that the motion-prediction module correctly estimates the motion of each object. This can be directly enforced in 3D space, or in image (perspective) space if a depth prediction module is utilized.

### 3.2. Collective Training of Tasks

Given a set of tasks  $\mathcal{T} = \{t_1, \dots, t_n\}$  we define losses for supervising each task individually, which we denote as  $\mathcal{L}_i^{sup}$ , as well as consistency losses for the collective training of sets of tasks, defined as  $\mathcal{L}^{con}$ . In the following tasks are referred to by their index  $i$ . We then define the overall loss as follows:

$$\mathcal{L} = \sum_{i=1}^n \mathcal{L}_i^{sup} \left( \hat{y}_i(w_i, x), x \right) + \mathcal{L}^{con} \left( \hat{y}_1(w_1, x), \hat{y}_2(w_2, x), \dots, \hat{y}_n(w_n, x) \right), \quad (1)$$

where  $\hat{y}_i(\cdot)$  denotes the generated prediction based on the weights  $w_i$  of a task  $i$  and  $x$  is a data sample. Consistency losses may not necessarily be defined for all task combinations, but only for those that are related in meaningful ways.

We assume that each task is performed by a separate deep network accompanied by a labeled dataset, which we refer to as its *dedicated dataset*. Furthermore, we use the standard supervision loss and separate datasets for each model as if we wanted to train them in isolation. For collective training we then use a third (unlabeled) dataset, which we refer to as *mediator dataset*, to enforce consistency between the tasks. During training, both tasks receive samples from the mediator dataset and the results of this forward pass are used to compute the consistency loss. The training loop of each tasks alternates by drawing samples from the dedicated and the mediator dataset. The setup for the collective training of two tasks is illustrated in Fig. 1.

The setup described above can have a few special cases: for one, a dedicated dataset for either task, or all, can be empty. In this case the setup reduces to unsupervised training; the unsupervised learning of depth and egomotion based on photometric consistency as a loss [86] exemplifies this case. Furthermore, datasets can overlap; i.e. a dataset can have labels for multiple tasks (e.g. for semantic segmentation and depth).

Similarly, the setup naturally generalizes to the collective training of  $N$  tasks, where the consistency loss is generally a function of the predictions of all participating tasks.

### 3.3. Distributed Collective Training

Collective training of multiple deep networks eventually requires distributing the computation across multiple compute nodes, to speed up the training, or simply because a large enough collection of models cannot be processed on a single machine. In distributed training it is often the communication between the nodes that sets the limitations. Either the models (data-parallelism) or their parts (model-parallelism) need to be synchronized, which increases the communication load as models become more complex. To reduce the communication load, distributed training schemes often aim to be asynchronous, which

means that model parameters or their gradient updates develop some degree of staleness. The more resilient an algorithm is to staleness, the less communication between nodes is necessary, which – in turn – improves scalability.

Online distillation [2] is a data parallelism paradigm that relies on the observation that stale labels are less harmful than stale gradient updates. By design, predictions are expected to converge as the training progresses; models that do not converge with respect to their predictions are not useful. Therefore, as the training progresses, the differences in the predictions produced by fresh and stale models will differ less and less. However, the latter is not necessarily true for weights, and even less so for gradients.

Our implementation of distributed training described in Sec. 3.2 follows the same principle. Each module is training on a separate machine (“trainer”), as illustrated in Fig. 3. The consistency loss depends on the outputs of all co-training tasks, which means that its computation requires evaluating a forward pass through all of them. Each trainer evaluates the forward pass of its own module and, to evaluate the forward passes of the other modules, it queries servers that host stale copies of the peer modules. At each training step, the trainer then pushes gradients to its own module and updates its weights. Furthermore, we define an update frequency to refresh the *forward-pass servers* with an updated copy of the respective module (copied from their trainers). We refer to the time interval between updates as “staleness”, which can be measured in wall time or in training steps.

We refer to *forward-pass servers* – as opposed to *inference servers* – to emphasize that a server performs a forward pass in training mode rather than in inference mode. Many models rely on different settings for the forward pass in training and during inference; e.g. models that use batch-normalization or dropout. Our experiments show that performing a forward pass in training mode can be crucial for successful co-training.

Another advantage of our distributed method is that each module can train with its own hyperparameters, including optimizer, regularizers, and learning rate schedules. Typically per-task modules are published together with these hyper-parameters, and our method allows using them as necessary for each respective model. Finally, since the modules communicate through predictions, and predictions are typically much more lightweight than network weights, the communication overhead is significantly lower compared to other distributed training techniques.

## 4. Experiments

In the following sections we report results of experiments on using consistency losses, for the distributed co-training of multiple models, reducing labels for supervi-

sion, domain adaptation, for exploring consistency losses for semantic segmentation, and object detection in point clouds. For all experiments we use existing model architectures along with the datasets, hyperparameters, and training specifications as detailed for each respective method. The specific consistency constraints used in each experiment are explained at high level, whereas detailed expressions are provided in the Appendix. The experiments in Sections 4.1, 4.2, and 4.5 were run distributed, as described in Sec. 3.3, whereas the rest of the experiments were run on a single machine, as shown in Fig. 1.

### 4.1. Distributed Collective Training of 3 Tasks

For this experiment we show results for the distributed collective training of three tasks. The first task is semantic segmentation based on NAS-FPN [30]. The other two tasks are depth prediction and motion estimation (camera and objects), for which we rely on existing models [34]. Segmentation masks were used to regularize the 3D motion fields [34]. This allows the 3D translation fields to deviate from their background value (due to camera motion) only at pixels that belong to possibly-moving objects (e.g. vehicles, pedestrians). Therefore, semantic segmentation informs 3D motion prediction, which has been shown to improve depth prediction [9, 32]. Conversely, given a depth map and a 3D motion field, optical flow fields can be derived and then used to assert the consistency of segmentation masks in pairs of adjacent frames. The flow fields can then be used to inform training of a semantic segmentation module. The formal definition of these consistency losses is given in the Appendix.

Semantic segmentation was trained on COCO [51] 2017 as its dedicated dataset and Cityscapes [14] was used as the unlabeled mediator dataset – no Cityscapes labels were used. Each of the three models was trained on a separate machine, as outlined in Sec. 3.3 and Fig. 3. The batch size, the optimizer, the learning rate, and other hyperparameters varied across the tasks and based on the respective published values for each model. During training each of the three models queries its peers via RPC to obtain their predictions, which were up to *one minute* stale.

The effect of collective training on the performance of the participating models is shown in Tab. 1. Experiments A and B are the baselines, where the depth and motion models were trained jointly, but separately from segmentation. Experiment E shows the improvement in performance when all three tasks train jointly with consistency constraints. Rows C and D are ablations that demonstrate the changes in performance when consistency constraints are turned on progressively. In C the depth and motion models are peer-supervised by the segmentation model from experiment B. C achieves the same depth error as a similar

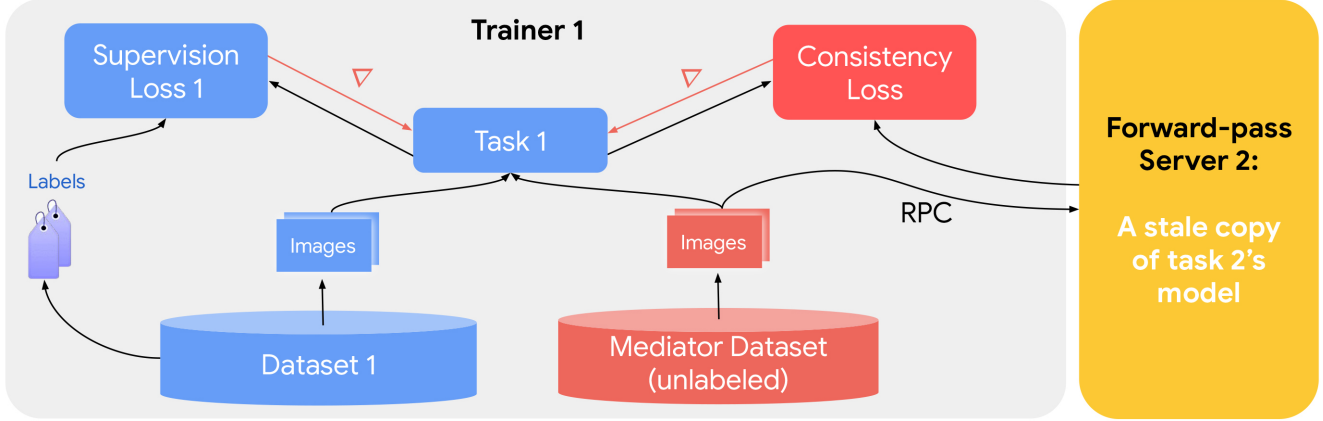


Figure 3. Illustration of our distributed setup for collective training. Each task-module is training on its own machine (its “trainer”, only Trainer 1 is shown in the figure). In order to compute the consistency loss, Trainer 1 reaches out to a server that hosts a stale copy of Task 2’s model and performs the forward pass (and vice versa). Each trainer pushes gradient updates to its respective model, and every so often, the stale copies on both forward-pass servers are refreshed with fresh copies from the respective trainer.

Configuration	Depth Error (Abs. Rel.)	Segmentation MIOU
A. Depth & motion only	0.165	-
B. Segmentation only	-	0.455
C. Frozen segmentation model B with depth & motion	0.129	-
D. Frozen depth & motion model C & segmentation	-	0.471
E. Depth, motion and segmentation training jointly	<b>0.125</b>	<b>0.478</b>

Table 1. Results of the distributed collective training of three models: Depth prediction, 3D motion prediction, and semantic segmentation. COCO was the dedicated dataset for semantic segmentation, and Cityscapes served as an unlabeled mediator dataset. Both depth prediction and segmentation were evaluated on Cityscapes, with segmentation evaluated only for predictions associated with pedestrians and vehicles (details of the evaluation protocol are given in the Appendix).

configuration trained on a single machine [34], where segmentation masks were precomputed. In experiment D, segmentation was peer-supervised by the improved depth and motion model from experiment C, but the latter two models remained frozen. The progression in quality demonstrates the effect of peer-supervision on all tasks.

#### 4.2. Improving 3D Detection in Point Clouds through Collective Training

In this section, we study object detection from 3D point clouds, a difficult task which also is crucial in many practical applications such as for autonomous vehicles. We show that if we simultaneously train an object flow network, which predicts motion of objects through time, we can apply a motion-consistency loss to significantly boost

the single-frame 3D object detector performance. We illustrate our setup in Fig. 4 (a).

Our backbone architecture is based on a PointPillar detector [50]. Given a sequence of input point clouds, we quantize the points for each frame into a grid in the  $x$ - $y$  plane and then use our single-frame detection model (M1) to produce a confidence value at each grid point for the presence of an object box as well as residual values  $(x, y, z, w, \ell, h, \theta)$  to refine the final box coordinates.

We can also use the same backbone to predict box flow. Namely, through an equivalent backbone we predict a three-channel map  $(dx, dy, d\theta)$  of the same resolution of the detector predictions, corresponding to the flow of the boxes in a current frame to any of the previous frames in the sequence (M2). The flow is only supervised at locations within the grid associated with positive object detections. This flow induces two natural consistency constraints with respect to the detection:

1.  $\mathcal{L}_{\text{class}}$ : The class confidences at two points  $(x, y, z) \mapsto (x + \text{flow}_x, y + \text{flow}_y, \theta + \text{flow}_\theta)$  connected by the predicted flow vector should have the same class confidence.
2.  $\mathcal{L}_{\text{residual}}$ : The predicted flow can be used to calculate consistent residual values for  $(x, y, \theta)$  at two points connected by the predicted flow. The residual values for  $z, w, \ell$ , and  $h$  should also remain constant between two detections connected by flow (for short time spans we assume near-constant elevation).

Overall, our motion-consistency loss becomes  $\mathcal{L}^{\text{con}} = \mathcal{L}_{\text{class}} + \mathcal{L}_{\text{residual}}$  as shown in Figure 4 (a). For more details on the exact architecture and mathematical formulae for our consistency loss, please refer to the Appendix



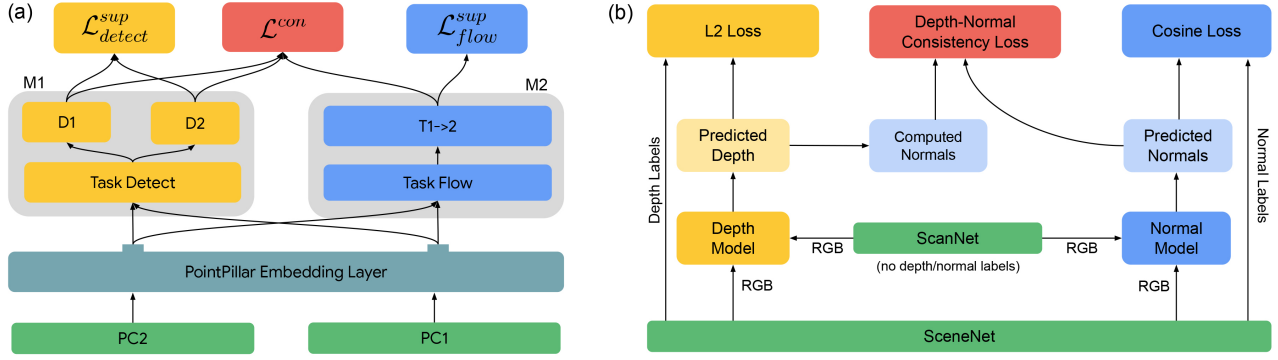


Figure 4. (a): Detection and flow estimation co-training: we use parts of Waymo OpenDataset to supervise the training of a single-frame detector (M1) and multi-frame flow estimator (M2) and apply a motion consistency loss on a set of unlabeled data. (b): Depth and normal co-training for domain adaptation: we use SceneNet data to supervise the training of separate models for depth and surface normal prediction and apply a consistency loss to jointly train both models for images from ScanNet, where we do not use any ground truth labels.

Method	Labels	3D mAP/mAPH (%)	BEV mAP/mAPH (%)
No Consistency	5%	17.6/9.6	44.3/24.3
Adding $\mathcal{L}^{con}$	5%	<b>23.5/12.0</b>	<b>51.1/26.5</b>
No Consistency	20%	30.8/16.4	63.0/34.1
Adding $\mathcal{L}^{con}$	20%	<b>31.6/19.1</b>	<b>65.7/39.2</b>
No Consistency	100%	53.0/47.6	75.0/66.8
Adding $\mathcal{L}^{con}$	100%	<b>54.2/49.6</b>	<b>75.0/68.5</b>

Table 2. 2D (BEV) and 3D detection metrics given various degrees of dataset labels provided for training. We can see consistent improvements when applying our motion-based consistency loss.

We perform all experiments on the vehicle class of the Waymo Open Dataset [72] which provides complete tightly-fitting 3D bounding box annotations along with tracks for each vehicle, and use a sequence length of three point clouds ( $\Delta = 0.5s$ ). Our main results are shown in Table 2. We present three sets of experiments, in which we stripped the dataset of its labels to various degrees. Our metrics are based on the standard mean average precision (mAP) metrics for 2D/3D detection. We also use the mAPH metric introduced in [72], which takes into account object heading. mAPH is calculated similarly to mAP, but all true positives are scaled by  $\text{err}_\theta/\pi$ , with  $\text{err}_\theta$  being the absolute angle error of the prediction in radians.

We thus have demonstrated that the motion-consistency loss improves detector performance in all three settings, with more significant improvements when labels are scarce. It is furthermore quite natural that the consistency loss has a significant beneficial effect on mAPH, as it enforces rotational consistency along each object track.

### 4.3. Consistency as an Alternative to Direct Supervision

Here we explore the capability of consistency constraints to compensate for missing labels. Specifically, we compare direct supervision through labels to peer-supervision

Fraction of Labels	MIOU	
	No CC	With CC
0.2%	43.2%	46.1%
0.5%	47.0%	49.4%
2%	49.1%	51.1%
4%	51.1%	51.1%

Table 3. Mean intersection over union (MIOU) of semantic segmentation models trained on ScanNet with partial supervision (i. e. with all but a small fraction of images stripped of their labels). The effect of joint training with depth and egomotion estimation and geometric consistency constraints (CC) as an additional supervision signal is shown in the rightmost column. No improvement in the MIOU was observed above a labeling fraction of 4%, due to the strong correlations between the ScanNet images.

through geometric consistency. We used the ScanNet dataset [15], which has annotations for semantic segmentation of 2.5M images captured in sequences in 1513 indoor scenes. We jointly trained semantic segmentation, depth estimation, and egomotion estimation.

The depth and egomotion estimation networks were trained unsupervised [86]. As described in Sec. 4.1, the consistency constraint for segmentation was imposed on pairs of adjacent frames; the motion-warped masks predicted for frame 1 have to correspond with the masks predicted for frame 2, and vice versa. The warping was calculated from the depth and egomotion prediction.

To test the ability of consistency constraints to compensate for missing labels, we only use a small fraction of labeled images from ScanNet and removed the labels from all others. A semantic segmentation network [30] was trained on the partially-labeled training set, with and without consistency constraints. The results of this experiment are summarized in Table 4.3: we observe that peer supervision through consistency constraints can mimic an increase in the number of labels by up to a factor of 4.

#### 4.4. Collective Training with Domain Disparity

Since training in our framework involves multiple datasets, it is interesting to explore what happens when there is a large domain disparity between them. To this end, we selected the extreme case of domain disparity between the dedicated datasets and the mediator dataset. As tasks for this experiment we selected depth estimation and surface normal prediction. We use SceneNet [56] (simulated data) as the dedicated dataset, and ScanNet [15] (real data) as the unlabeled mediator dataset. We use SceneNet to train depth and normal estimation models and evaluate them on the ScanNet data as our baseline. The strong domain disparity is evident from the fact that a model trained on simulated data performs poorly on the real dataset. We then train the models with consistency loss on ScanNet, and observe that it improves the performance on both tasks.

For the baseline both models are trained separately to predict depth and surface normals, with a mean squared error loss for the depth model and a cosine loss for the surface normal model. The trained models are then used to predict surface normals for samples from ScanNet. For co-training we use our depth network to predict depth and analytically compute the surface normals based on the derivatives of the generated depth map [45]. The consistency loss can then be computed as cosine similarity of the computed surface normals and those predicted by the normal prediction network (an explicit expression is given in the Appendix). Accuracy is measured by using the ground truth data of ScanNet for depth and surface normals generated by the method of [37].

Figure 4 (b) shows the training setup for both networks trained with consistency loss. Table 4.4 shows the results for surface normal prediction and depth estimation of data from ScanNet with models trained on SceneNet with and without consistency loss.

Method	Normals Accuracy (in %)			Depth Error (in %)
	< 11.25°	< 22.50°	< 30.00°	Abs. Rel
SceneNet → ScanNet	9.2	30.8	46.3	28.2
SceneNet → ScanNet (with Consistency)	<b>13.6</b>	<b>34.9</b>	<b>46.7</b>	<b>24.9</b>

Table 4. Surface normal prediction transfer from SceneNet (simulated) to ScanNet (real).

#### 4.5. Tolerance to Staleness

As discussed in Sec. 3.3, in our setup individual modules communicate with each other through their predictions. This is motivated by the increased resilience to staleness that predictions exhibit compared to weights and gradients [2]. To study the amount of staleness our setup can afford, we train depth and egomotion [9] on KITTI, each on a separate machine. This experiment is particularly challenging because it is fully unsupervised: each of the two modules is only supervised by the predictions produced by

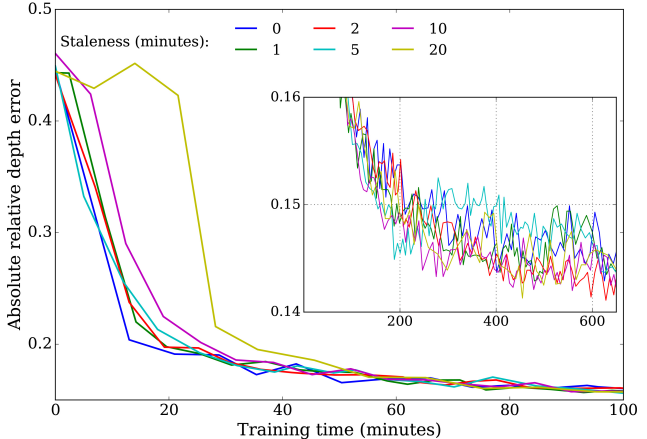


Figure 5. Depth prediction error as function of time for different values of staleness for distributed collective training on depth and egomotion on KITTI. Staleness of 20 minutes means that the depth trainer receives egomotion labels from an egomotion model that refreshes every 20 minutes, and vice versa. The depth trainer performs about 100 training steps per minute, so 20 minutes translates to 2000 steps. A value of 0 staleness denotes a configuration where all networks were placed on the same machine and trained synchronously. The graphs in the inset show the long-time progression of training. All experiments achieve the same absolute relative depth prediction error of about 0.143 (which on is par with the state-of-the-art [9] for models that disregard object motion), at about the same time, irrespectively of the staleness.

its peer. Since both modules are randomly initialized each model initially receives a *random* and *stale* peer-supervision signal.

In Fig. 5 we show the results of this experiment, which is the depth prediction error as function of time for various values of staleness. While greater staleness values initially hinder the training, all experiments converge to approximately the same result, and approximately at the same time. Staleness of up to 20 minutes – or 2000 training steps – is shown to have no adverse effect on the convergence time or the test metric.

The negative effects of staleness on convergence time and on result metrics have been studied for various distributed training methods [16, 11, 10, 23]. While the tolerance to staleness varies widely, due to the diversity of methods, most studies only report the sensitivity of methods to staleness of up to a few tens of steps. Unlike these findings, our distributed training setup is much more robust and thereby enables training with staleness of up to thousands of steps.

In this experiment two modules were training jointly, depth estimation and egomotion estimation. The modules and losses are exactly the same one as in Sec. A.3, except that this experiment did not include a segmentation model, and hence no segmentation consistency losses:  $\mathcal{L}_{\text{con-photo}}$  was the only loss (see A.1.2, Eq. 5 for details).



## 5. Discussion, Limitations, and Future Work

We have introduced a novel framework for the collective training of multiple models of different computer vision tasks. Our main contribution is that our framework enables a modular design for training neural networks by separating tasks into modules that can be combined and trained collectively. Furthermore, we employ consistency losses so as to exploit the structure between tasks. By jointly training multiple tasks, we have shown that consistency losses help to improve the performance of existing neural network architectures. Unlike model- or data-parallelism, our approach allows us to split the training at tasks level, which directly enables the training of large model collections at scale and in a distributed manner.

While our framework offers many advantages, our current setup also has a number of limitations. Our framework prioritizes minimum engineering effort and maximum scalability in combining tasks. This general setup may not always generate the best possible performance or the lowest possible compute cost, on any given combination of tasks; a specialized solution with a well-tuned set of hyperparameters may arguably yield higher performance. However, highly specialized solutions are more likely to incur greater engineering costs in designing and maintaining them, thereby slowing down research and development.

While we have not exhaustively explored all facets of our framework, it appears to offer advantages for multi-task training. For one, it allows us to develop more complex architectures that are better suited for individual tasks. Second, a modular design for neural networks allows us to disentangle the intricacies of training multi-tasks models, such as finding joint hyperparameters or datasets. Finally, individual models can be trained jointly on different compute units, which enables training large collections of models simultaneously. As our framework is not limited to computer vision tasks, we see many possibilities for collective training, e.g. as found for tasks in visual question answering, natural language processing, or audio and video synchronization, which we would like to address as future work. Another avenue for future work is to further explore the collective training of tasks and model combinations. For example, imposing consistency constraints between point clouds and perspective views (images) seems like a promising direction for future research.

## References

- [1] E. Ahmed, A. Saint, A. E. R. Shabayek, K. Cherenkova, R. Das, G. Gusev, D. Aouada, and B. E. Ottersten. Deep learning advances on different 3d data representations: A survey. *ArXiv*, 2018.
- [2] R. Anil, G. Pereyra, A. Passos, R. Ormandi, G. E. Dahl, and G. E. Hinton. Large scale distributed neural network training through online distillation. In *ICLR*, 2018.
- [3] Y. Aytar and A. Zisserman. Tabula rasa: Model transfer for object category detection. In *ICCV*, pages 2252–2259, 2011.
- [4] Y. Bengio, A. Courville, and P. Vincent. Representation learning: A review and new perspectives. *TPAMI*, 2013.
- [5] P. Berkhin. *A Survey of Clustering Data Mining Techniques*, pages 25–71. Springer Berlin Heidelberg, 2006.
- [6] H. Bilen and A. Vedaldi. Integrated perception with recurrent multi-task neural networks. In *NIPS*, pages 235–243. 2016.
- [7] A. Byravan and D. Fox. Se3-nets: Learning rigid body motion using deep neural networks. 2017.
- [8] R. Caruana. Multitask learning: A knowledge-based source of inductive bias. In *ICML*, page 4148, 1993.
- [9] V. Casser, S. Pirk, R. Mahjourian, and A. Angelova. Depth prediction without the sensors: Leveraging structure for unsupervised learning from monocular videos. In *AAAI*, volume 33, pages 8001–8008, 2019.
- [10] C.-C. Chen, C.-L. Yang, and H.-Y. Cheng. Efficient and robust parallel dnn training through model parallelism on multi-gpu platform, 2018.
- [11] J. Chen, X. Pan, R. Monga, S. Bengio, and R. Jozefowicz. Revisiting distributed synchronous sgd, 2016.
- [12] Z. Chen, V. Badrinarayanan, C.-Y. Lee, and A. Rabinovich. Gradnorm: Gradient normalization for adaptive loss balancing in deep multitask networks. In *International Conference on Machine Learning*, pages 794–803, 2018.
- [13] J. Cheng, Y. Tsai, S. Wang, and M. Yang. Segflow: Joint learning for video object segmentation and optical flow. In *ICCV*, pages 686–695, 2017.
- [14] M. Cordts, M. Omran, S. Ramos, T. Rehfeld, M. Enzweiler, R. Benenson, U. Franke, S. Roth, and B. Schiele. The cityscapes dataset for semantic urban scene understanding. In *CVPR*, 2016.
- [15] A. Dai, A. X. Chang, M. Savva, M. Halber, T. Funkhouser, and M. Nießner. Scannet: Richly-annotated 3d reconstructions of indoor scenes. In *CVPR*, 2017.
- [16] W. Dai, Y. Zhou, N. Dong, H. Zhang, and E. P. Xing. Toward understanding the impact of staleness in distributed machine learning, 2018.
- [17] J. Dean, G. S. Corrado, R. Monga, K. Chen, M. Devin, Q. V. Le, M. Z. Mao, M. Ranzato, A. Senior, P. Tucker, K. Yang, and A. Y. Ng. Large scale distributed deep networks. 2012.
- [18] T. Dharmasiri, A. Spek, and T. Drummond. Joint prediction of depths, normals and surface curvature from RGB images using cnns. *CoRR*, 2017.
- [19] C. Doersch, A. Gupta, and A. A. Efros. Unsupervised visual representation learning by context prediction. In *ICCV*, page 14221430, 2015.
- [20] C. Doersch and A. Zisserman. Multi-task self-supervised visual learning. *CoRR*, 2017.
- [21] J. Donahue, P. Krähenbühl, and T. Darrell. Adversarial feature learning. *ArXiv*, 2016.
- [22] A. Dosovitskiy, P. Fischer, E. Ilg, P. Häusser, C. Hazirbas, V. Golkov, P. van der Smagt, D. Cremers, and T. Brox. FlowNet: Learning optical flow with convolutional networks. *ICCV*, pages 2758–2766, 2015.
- [23] S. Dutta, G. Joshi, S. Ghosh, P. Dube, and P. Nagpurkar. Slow and stale gradients can win the race: Error-runtime trade-offs in distributed sgd, 2018.

- [24] D. Eigen, C. Puhrsch, and R. Fergus. Depth map prediction from a single image using a multi-scale deep network. In *NIPS*, pages 2366–2374, 2014.
- [25] D. Erhan, C. Szegedy, A. Toshev, and D. Anguelov. Scalable object detection using deep neural networks. In *CVPR*, pages 2155–2162, 2014.
- [26] B. Fernando, A. Habrard, M. Sebban, and T. Tuytelaars. Unsupervised visual domain adaptation using subspace alignment. In *ICCV*, page 29602967, 2013.
- [27] V. Fischer, J. Koehler, and T. Pfeil. The streaming rollout of deep networks - towards fully model-parallel execution. In S. Bengio, H. Wallach, H. Larochelle, K. Grauman, N. Cesa-Bianchi, and R. Garnett, editors, *NIPS*, pages 4039–4050, 2018.
- [28] I. Fodor. A survey of dimension reduction techniques. Technical report, Lawrence Livermore National Lab, CA (US), 2002.
- [29] D. F. Fouhey, A. Gupta, and M. Hebert. Data-driven 3d primitives for single image understanding. In *ICCV*, pages 3392–3399, 2013.
- [30] G. Ghiasi, T.-Y. Lin, and Q. V. Le. Nas-fpn: Learning scalable feature pyramid architecture for object detection. In *The IEEE Conference on Computer Vision and Pattern Recognition (CVPR)*, June 2019.
- [31] C. Godard, O. M. Aodha, and G. J. Brostow. Unsupervised monocular depth estimation with left-right consistency. *CVPR*, 2017.
- [32] C. Godard, O. Mac Aodha, M. Firman, and G. J. Brostow. Digging into self-supervised monocular depth estimation. In *ICCV*, 2019.
- [33] R. Gopalan, Ruonan Li, and R. Chellappa. Domain adaptation for object recognition: An unsupervised approach. In *ICCV*, pages 999–1006, 2011.
- [34] A. Gordon, H. Li, R. Jonschkowski, and A. Angelova. Depth from videos in the wild: Unsupervised monocular depth learning from unknown cameras. In *ICCV*, 2019.
- [35] Y. Guo, H. Wang, Q. Hu, H. Liu, L. Liu, and M. Bennamoun. Deep learning for 3d point clouds: A survey. *arXiv*, 2019.
- [36] K. He, G. Gkioxari, P. Dollr, and R. Girshick. Mask r-cnn. In *ICCV*, pages 2980–2988, 2017.
- [37] S. Hickson, K. Raveendran, A. Fathi, K. Murphy, and I. A. Essa. Floors are flat: Leveraging semantics for real-time surface normal prediction. *CoRR*, 2019.
- [38] G. Hinton, O. Vinyals, and J. Dean. Distilling the knowledge in a neural network. *arXiv*, 2015.
- [39] J. Hoffman, T. Darrell, and K. Saenko. Continuous manifold based adaptation for evolving visual domains. In *CVPR*, page 867874, 2014.
- [40] T.-W. Hui, X. Tang, and C. C. Loy. Liteflownet: A lightweight convolutional neural network for optical flow estimation. In *CVPR*, 2018.
- [41] L. Jiao, F. Zhang, F. Liu, S. Yang, L. Li, Z. Feng, and R. Qu. A survey of deep learning-based object detection. *IEEE Access*, pages 128837–128868, 2019.
- [42] X. Jin, X. Li, H. Xiao, X. Shen, Z. Lin, J. Yang, Y. Chen, J. Dong, L. Liu, Z. Jie, J. Feng, and S. Yan. Video scene parsing with predictive feature learning. In *ICCV*, pages 5581–5589, 2017.
- [43] A. Kendall, Y. Gal, and R. Cipolla. Multi-task learning using uncertainty to weigh losses for scene geometry and semantics. In *Proceedings of the IEEE conference on computer vision and pattern recognition*, pages 7482–7491, 2018.
- [44] D. P. Kingma and M. Welling. Auto-encoding variational bayes. In Y. Bengio and Y. LeCun, editors, *ICLR*, 2014.
- [45] K. Klasing, D. Althoff, D. Wollherr, and M. Buss. Comparison of surface normal estimation methods for range sensing applications. In *ICRA*, pages 3206–3211, 2009.
- [46] I. Kokkinos. Ubernet: Training a ‘universal’ convolutional neural network for low-, mid-, and high-level vision using diverse datasets and limited memory. *CoRR*, 2016.
- [47] A. Krizhevsky. One weird trick for parallelizing convolutional neural networks. *CoRR*, 2014.
- [48] B. Kulis, K. Saenko, and T. Darrell. What you saw is not what you get: Domain adaptation using asymmetric kernel transforms. In *CVPR*, pages 1785–1792, 2011.
- [49] A. C. S. Kumar, S. M. Bhandarkar, and M. Prasad. Depthnet: A recurrent neural network architecture for monocular depth prediction. In *CVPRW*, pages 396–3968, 2018.
- [50] A. H. Lang, S. Vora, H. Caesar, L. Zhou, J. Yang, and O. Beijbom. Pointpillars: Fast encoders for object detection from point clouds. In *CVPR*, pages 12697–12705, 2019.
- [51] T.-Y. Lin, M. Maire, S. Belongie, J. Hays, P. Perona, D. Ramanan, P. Dollár, and C. L. Zitnick. Microsoft coco: Common objects in context. In *ECCV*, pages 740–755, 2014.
- [52] P. Luc, N. Neverova, C. Couprie, J. Verbeek, and Y. LeCun. Predicting deeper into the future of semantic segmentation. *ICCV*, 2017.
- [53] J. Malik, P. Arbelaz, J. Carreira, K. Fragkiadaki, R. Girshick, G. Gkioxari, S. Gupta, B. Hariharan, A. Kar, and S. Tulsiani. The three rs of computer vision: Recognition, reconstruction and reorganization. *Pattern Recognition Letters*, pages 4 – 14, 2016.
- [54] R. Mayer and H.-a. Jacobsen. Scalable deep learning on distributed infrastructures: Challenges, techniques, and tools. *ACM Computing Surveys (CSUR)*, pages 1–37, 2020.
- [55] R. Mayer, C. Mayer, and L. Laich. The tensorflow partitioning and scheduling problem: Its the critical path! In *Proceedings of the 1st Workshop on Distributed Infrastructures for Deep Learning*, page 16, 2017.
- [56] J. McCormac, A. Handa, S. Leutenegger, and A. J. Davison. Scenenet rgb-d: Can 5m synthetic images beat generic imagenet pre-training on indoor segmentation? 2017.
- [57] A. Mirhoseini, A. Goldie, H. Pham, B. Steiner, Q. V. Le, and J. Dean. A hierarchical model for device placement. In *ICLR*, 2018.
- [58] A. Mirhoseini, H. Pham, Q. V. Le, B. Steiner, R. Larsen, Y. Zhou, N. Kumar, M. Norouzi, S. Bengio, and J. Dean. Device placement optimization with reinforcement learning. In *ICML*, page 24302439, 2017.
- [59] I. Misra, A. Shrivastava, A. Gupta, and M. Hebert. Cross-stitch networks for multi-task learning. *CVPR*, pages 3994–4003, 2016.
- [60] M. Noroozi and P. Favaro. Unsupervised learning of visual representations by solving jigsaw puzzles. In B. Leibe, J. Matas, N. Sebe, and M. Welling, editors, *ECCV*, pages 69–84, 2016.

- [61] M. Noroozi, H. Pirsiavash, and P. Favaro. Representation learning by learning to count. *CoRR*, 2017.
- [62] D. Pathak, P. Krähenbühl, J. Donahue, T. Darrell, and A. Efros. Context encoders: Feature learning by inpainting. *CVPR*, 2016.
- [63] A. Pentina and C. H. Lampert. Multi-task learning with labeled and unlabeled tasks. In *ICML*, page 28072816, 2017.
- [64] X. Qi, R. Liao, Z. Liu, R. Urtasun, and J. Jia. Geonet: Geometric neural network for joint depth and surface normal estimation. In *CVPR*, 2018.
- [65] Z. Ren, J. Yan, B. Ni, B. Liu, X. Yang, and H. Zha. Unsupervised deep learning for optical flow estimation. In *AAAI*, page 14951501, 2017.
- [66] S. R. Richter, Z. Hayder, and V. Koltun. Playing for benchmarks. In *ICCV*, pages 2232–2241, 2017.
- [67] S. T. Roweis and L. K. Saul. Nonlinear dimensionality reduction by locally linear embedding. *Science*, (5500):2323–2326, 2000.
- [68] S. Ruder. An overview of multi-task learning in deep neural networks. *CoRR*, 2017.
- [69] K. Saenko, B. Kulis, M. Fritz, and T. Darrell. Adapting visual category models to new domains. In *ECCV*, page 213226, 2010.
- [70] O. Sener and V. Koltun. Multi-task learning as multi-objective optimization. In *Advances in Neural Information Processing Systems*, pages 527–538, 2018.
- [71] S. Shalev-Shwartz and A. Shashua. On the sample complexity of end-to-end training vs. semantic abstraction training. *CoRR*, 2016.
- [72] P. Sun, H. Kretzschmar, X. Dotiwalla, A. Chouard, V. Patnaik, P. Tsui, J. Guo, Y. Zhou, Y. Chai, B. Caine, V. Vasudevan, W. Han, J. Ngiam, H. Zhao, A. Timofeev, S. Ettinger, M. Krivokon, A. Gao, A. Joshi, Y. Zhang, J. Shlens, Z. Chen, and D. Anguelov. Scalability in perception for autonomous driving: Waymo open dataset. In *Proceedings of the IEEE Conference on Computer Vision and Pattern Recognition*, 2020.
- [73] C. Tessler, S. Givony, T. Zahavy, D. J. Mankowitz, and S. Mannor. A deep hierarchical approach to lifelong learning in minecraft. In *AAAI*, page 15531561, 2017.
- [74] A. M. Turing. Computing machinery and intelligence. (236):433–460, 1950.
- [75] P. Wang, X. Shen, B. Russell, S. Cohen, B. Price, and A. L. Yuille. Surge: Surface regularized geometry estimation from a single image. *NIPS*, pages 172–180, 2016.
- [76] X. Wang, K. He, and A. Gupta. Transitive invariance for self-supervised visual representation learning. *CoRR*, 2017.
- [77] T. Winograd. *Thinking Machines: Can There Be? Are We?*, page 167189. Cambridge University Press, USA, 1990.
- [78] Y. Wu, M. Schuster, Z. Chen, Q. V. Le, M. Norouzi, W. Macherey, M. Krikun, Y. Cao, Q. Gao, K. Macherey, et al. Google’s neural machine translation system: Bridging the gap between human and machine translation. 2016.
- [79] E. P. Xing, Q. Ho, W. Dai, J. K. Kim, J. Wei, S. Lee, X. Zheng, P. Xie, A. Kumar, and Y. Yu. Petuum: A new platform for distributed machine learning on big data. *IEEE Transactions on Big Data*, 1(2):49–67, 2015.
- [80] J. Yang, R. Yan, and A. G. Hauptmann. Adapting svm classifiers to data with shifted distributions. In *ICDMW*, pages 69–76, 2007.
- [81] A. Zamir, A. Sax, W. Shen, L. Guibas, J. Malik, and S. Savarese. Taskonomy: Disentangling task transfer learning. pages 3712–3722, 06 2018.
- [82] A. R. Zamir, T. Wekel, P. Agrawal, C. Wei, J. Malik, and S. Savarese. Generic 3d representation via pose estimation and matching. In *ECCV*, 2016.
- [83] H. Zhan, C. S. Weerasekera, R. Garg, and I. D. Reid. Self-supervised learning for single view depth and surface normal estimation. *CoRR*, 2019.
- [84] R. Zhang, P. Isola, and A. A. Efros. Colorful image colorization. In *ECCV*, pages 649–666, 2016.
- [85] Y. Zhang and Q. Yang. A survey on multi-task learning. *CoRR*, 2017.
- [86] T. Zhou, M. Brown, N. Snaveley, and D. G. Lowe. Unsupervised learning of depth and ego-motion from video. In *CVPR*, pages 1851–1858, 2017.

## A. Appendix

In the main paper, we strived to demonstrate the generality of our method by applying it on a wide variety of combinations of tasks. This left limited space for details pertaining to each of the combinations, and specifically, the explicit form of the consistency loss for each combination could not be included. Here we provide explicit expressions for the consistency constraints used in each experiment in Sec. 4 of the paper, as well as certain implementation details. To enable modularity, we aim to formulate the consistency constraint so that it only depends on the outputs of the constituent tasks, and is agnostic to their implementations.

### A.1. Depth, Motion and Semantic Segmentation

#### A.1.1 Modules and Interfaces

The interfaces of the three modules, depth, motion and semantic segmentation, are defined below:

**Motion Prediction Network:** Given two consecutive RGB frames,  $I_1(i, j)$  and  $I_2(i, j)$ , of width  $w$  ( $0 \leq j < w$ ) and height  $h$  ( $0 \leq i < h$ ), the motion prediction network predicts the following quantities:

- $\delta t_{1 \rightarrow 2}(i, j)$ : For every pixel  $(i, j)$ ,  $\delta t_{1 \rightarrow 2}(i, j)$  estimates the movement of the point visible at the pixel  $(i, j)$  of frame 1, relative to the scene, which occurred between frame 1 and frame 2.
- $T_{1 \rightarrow 2}$ : The translation vector of the camera between frame 2 and frame 1.
- $R_{1 \rightarrow 2}$ : The rotation matrix of the camera between frame 2 and frame 1.

Similarly, the network predicts  $\delta t_{2 \rightarrow 1}(i, j)$ ,  $T_{2 \rightarrow 1}$ , and  $R_{2 \rightarrow 1}$ , which are defined as above, with (1) and (2) swapped.

**Depth Prediction Network:** Given an RGB frame,  $I(i, j)$ , the depth prediction network predicts a depth map,  $z(i, j)$ , for every pixel  $(i, j)$ .

**Semantic Segmentation Network:** Given an RGB frame,  $I(i, j)$ , the semantic segmentation network predicts a logit map  $l_c(i, j)$  for each class  $c$ . For each pixel  $(i, j)$ , the class is given by  $c(i, j) = \operatorname{argmax}_c l_c(i, j)$ .

#### A.1.2 Consistency Loss

To construct the loss, we start with defining  $m(i, j)$  to be the *movable mask*:

$$m(i, j) = \begin{cases} 1 & c(i, j) \in \mathcal{M} \\ 0 & \text{otherwise} \end{cases} \quad (2)$$

$\mathcal{M}$  is the collection of all classes that represent movable objects. These are detailed in Sec. A.1.3. For each pixel

$(i, j)$ ,  $m(i, j)$  equals 1 if the pixel belongs to one of the movable object classes, and 0 otherwise.

Given two adjacent video frames, 1 and 2, a depth map of frame 1  $z_1(i, j)$ , the camera matrix  $K$ , and a pixel position in homogeneous coordinates

$$p(i, j) = \begin{pmatrix} j \\ i \\ 1 \end{pmatrix}, \quad (3)$$

one can write the shift in  $p$  resulting from the rotation and a translation that occurred between the two frames as:

$$z'_1(i, j)p'_1(i, j) = KR_{1 \rightarrow 2}K^{-1}z_1(i, j)p_1(i, j) + K(m_1(i, j)t_{1 \rightarrow 2}(i, j) + T_{1 \rightarrow 2}), \quad (4)$$

where  $p'_1$  and  $z'_1$  are respectively the new homogeneous coordinates of the pixel and the new depth, projected onto frame 2. The movable mask  $m_1(i, j)$  (of frame 1) restricts motion of objects relative to the scene to occur only at pixels that belong to movable objects.

The first type of the consistency constraint utilized in this experiment is photometric consistency across adjacent frames. To formulate this constraint, we sample  $I_2(i, j)$  at the pixel positions  $p'_1(i, j)$ , and using bilinear interpolation, we obtain  $I'_1(i, j)$ , frame 2's RGB image warped onto frame 1. The photometric loss can then be written generally as

$$\mathcal{L}_{con.photo} = \sum_{i,j} \mathcal{L}_{ph}(I'_1(i, j), I_1(i, j)) + \sum_{i,j} \mathcal{L}_{ph}(I'_2(i, j), I_2(i, j)), \quad (5)$$

where  $I'_2$  is defined analogously to  $I'_1$ , just with 1 and 2 swapped everywhere.  $\mathcal{L}_{ph}$  stands for a pixelwise photometric loss, such as an L1 penalty on the difference in RGB space and structural similarity (SSIM), each weighed by a coefficient. In addition, both SSIM and the difference in RGB space can have different per-pixel weights, for example, to mask out pixels that become occluded or flow out of the frame. In our experiments we used the same photometric loss as described in [34].

The second type of the consistency constraint utilized in this experiment is segmentation logits consistency across adjacent frames. To formulate this constraint, we sample  $l_{c2}(i, j)$  at the pixel positions  $p'_1(i, j)$ , and using bilinear interpolation, we obtain  $l'_{c1}(i, j)$ . The segmentation consistency loss can then be written generally as

$$\mathcal{L}_{con.seg} = \sum_{i,j,c} \mathcal{L}_2(l'_{c1}(i, j), l_{c1}(i, j)) + \sum_{i,j,c} \mathcal{L}_2(l'_{c2}(i, j), l_{c2}(i, j)), \quad (6)$$

where  $l'_{c2}$  is defined analogously to  $l'_{c1}$ , just with 1 and 2 swapped everywhere.  $\mathcal{L}_2$  stands for a L2 loss squared.

Class	Label ID		
	Ours	COCO 2017	Cityscapes
person/rider	1	1	24/25
bicycle	2	2	33
car	3	3	26
motorcycle	4	4	32
traffic lights	5	10	19
bus	6	6	28
truck	7	8	27
others	8	any other label	any other label

Table 5. Mapping between Cityscapes label IDs, COCO labels IDs, and the label IDs we defined for this experiment.

### A.1.3 Movable Objects Classes and Segmentation Evaluation Protocol

In our experiment COCO served as the dedicated dataset for segmentation, and Cityscapes served as the unlabeled mediator dataset. Since the two datasets have different sets of labels, we had to create a mapping between the two. The mapping is shown in Table 5.

Only labels that represent movable objects are of interest for our experiment. We therefore restricted our label set to 7 classes, that are in the intersection of Cityscapes and COCO and represent movable objects. All other labels were mapped to label ID 8. When evaluating the segmentation on Cityscapes, we mapped the Cityscapes groundtruth labels and the COCO-trained model predictions to these 8 labels.

### A.2. Improving 3D Detection in Point Clouds through Collective Training

In this section, we formulate the motion-consistency loss in more detail, applied on two models: one predicting 3D bounding boxes on a point cloud, and the other predicting 2D box flow on point cloud sequences. Our detection model operates on the grid-voxelized input point cloud of shape  $(n_x, n_y)$ , where we choose  $n_x = n_y = 468$  (the  $z$  dimension has been marginalized out as we are using a PointPillar [50] model). The grid size in  $x - y$  corresponds to each grid point being of extent (0.32m, 0.32m) in real space. For each grid point, we predict:

1.  $(7n_a, n_f)$  residual values pinned to  $n_a$  fixed anchors. The 7 values correspond to  $dx, dy, dz, dw, dl, dh, d\theta$  of the final predicted box. Ground truth boxes are automatically corresponded to anchors at training time.  $n_f$  is the number of frames (in the given temporal sequence) for which we predict boxes.
2.  $(n_a, n_f)$  class logit values denoting confidence that an object of the specified type exists for that anchor box.
3.  $(3, n_f - 1)$  values corresponding to the box flow  $(flow_x, flow_y, flow_\theta)$  of a hypothetical box in the current frame to any  $n_f - 1$  frames in the past.

We use a PointPillar-based [50] network as our 3D detector, which allows us to work in a pseudo-2D top-down space for all our experiments. At the shared feature layer preceding the detector prediction head we attach a flow prediction head that outputs  $3(n_f - 1)$  channels corresponding to flow in each frame.

The flow is only supervised at locations within the grid associated with positive object detections. We perform all experiments on the vehicle class of the Waymo Open Dataset [72] which provides complete tightly-fitting 3D bounding box annotations along with tracks for each vehicle. For all our reported experiments,  $n_f = 3$  and  $n_a = 2$ . The two anchors are centered at the same spatial location but are 90 degree rotated from each other. We also follow the original PointPillar network settings in choosing all class thresholds. Our baseline (100%) is trained in isolation, whereas all partial label studies are performed in the distributed framework.

This set of detection and flow predictions induces a natural consistency measure. Namely, given a predicted flow that transforms an anchor point centered at  $(x, y)$  in the current frame to the closest anchor point  $(x + flow_x, y + flow_y, \theta + flow_\theta) \approx (x', y', \theta')$  in another frame, we consider the following two loss functions (in the following, all primed coordinates are coordinates after flow has been applied to the current frame):

$$\begin{aligned}
1. \mathcal{L}_{\text{con.class}} &= (\text{classlogit}(x, y) - \text{classlogit}(x', y'))^2 \\
2. \mathcal{L}_{\text{con.residual}} &= \sum_{i \in (x, y, \theta)} (di' - di + (\text{flow}_i - (i' - i))^2 + \\
&\quad \sum_{j \in (z, \ell, w, h)} (dj' - dj)^2
\end{aligned}$$

The class loss  $\mathcal{L}_{\text{class}}$  ensures that class logits along predicted object tracks are equal, while the residual loss  $\mathcal{L}_{\text{residual}}$  do the same for residual values along tracks. The first term in the residual consistency takes into account the predicted flow, which transforms  $(x, y, \theta)$  to  $(x', y', \theta')$ . Because the flow is continuous and not quantized like the voxel grid, we can normalize out the quantization noise exactly by adding a remainder term,  $(\text{flow}_i - (i' - i))$  for  $i \in (x, y, \theta)$ . For the residual consistency, we further enforce that the bounding box residuals for  $z, \ell, w, h$  do not change along object tracks. This reflects our assumption that the dimensions of the vehicle are preserved and there is no appreciable elevation change over the span of a second.

### A.3. Consistency as an Alternative to Direct Supervision

For this experiment, the interfaces of the three modules, i. e. depth, motion and semantic segmentation, are identical to the ones described in Sec. A.1, except for the motion prediction module. In this experiment object motion relative to the scene  $(\delta t_{1 \rightarrow 2}(i, j))$  is not predicted, and assumed to be zero. This is compatible with the dataset on which

the experiment was run (ScanNet), where all the scenes are static.

The photometric consistency loss employed in this set of experiments was identical to  $\mathcal{L}_{\text{ph}}$  referenced in Sec. A.1. The segmentation consistency loss was similar to Eq. 6, with the only difference that  $\mathcal{L}_2$  was replaced  $\mathcal{L}_s$ , defined below:

$$\mathcal{L}_s(l'_c(i, j), l_c(i, j)) = |l'_c(i, j) - l_c(i, j)| \cdot (\alpha + \beta \delta(c, c(i, j)) + \gamma \mathcal{E}(I(i, j))). \quad (7)$$

$\alpha$ ,  $\beta$ , and  $\gamma$  are coefficients,  $\delta(\cdot, \cdot)$  is the Kronecker delta,  $c(i, j) = \text{argmax}_c l_c(i, j)$ , and  $\mathcal{E}$  is an edge detector: A function that assigns larger values for pixels  $(i, j)$  that have a stronger contrast to their neighborhood.

The three terms in the parentheses on the right hand side of Eq. 7 provide different weighing for  $|l'_c(i, j) - l_c(i, j)|$  the L1 consistency loss in logit space. The first term weighs all pixels equally. The second term assigns nonzero weight only to the dominant class of each pixel. The rationale is that it is more important to assert consistency between the class that are present at a given pixel than for classes that are absent. The last term assigns more weights at edges, the rationale being that segmentation mask edges tend to co-occur with edges in RGB space, and thus asserting consistency of segmentation masks is more important there. In our experiments, we used  $\alpha = 0.2$ ,  $\beta = 0.4$ , and  $\gamma = 0.4$ . The edge detector operator  $\mathcal{E}$  was normalized such that the maximum value it can produce is 1.0.

#### A.4. Collective Training with Domain Disparity

To compute a consistency loss for the collective training of depth and normal prediction models we compute surface normals from the *predicted depth map*, and penalize their deviation from the *predicted normal map*. We first convert the the depth map to a 3D point cloud, using the inverse of the intrinsics matrix:

$$\vec{r}_{ij} \equiv \begin{pmatrix} x_{i,j} \\ y_{i,j} \\ z_{i,j} \end{pmatrix} = z_{i,j} \cdot \begin{pmatrix} 1/f_x & 0 & -x_0/f_x \\ 0 & 1/f_y & -y_0/f_y \\ 0 & 0 & 1 \end{pmatrix} \begin{pmatrix} j \\ i \\ 1 \end{pmatrix} \quad (8)$$

where  $f_x$  and  $f_y$  denote the focal length, and  $x_0$  and  $y_0$  the principal point offset,  $i$  and  $j$  are the pixel coordinates along the height and the width of the image respectively, and  $z_{ij}$  is the depth map evaluated at the pixel coordinates  $(i, j)$ .  $\vec{r}_{ij}$  is a point in 3D space, in the camera coordinates, corresponding to pixel  $(i, j)$ . We then compute the spatial derivatives of the depth map:

$$\begin{aligned} (\partial x, \vec{r})_{i,j} &= \vec{r}_{i,j+1} - \vec{r}_{i,j-1} \\ (\partial y, \vec{r})_{i,j} &= \vec{r}_{i+1,j} - \vec{r}_{i-1,j}. \end{aligned} \quad (9)$$

To exclude depth discontinuities, we invalidate pixels where the spatial gradient of the depth relative to the depth itself is

greater than a certain threshold  $\beta$ . To this end, we define a validity mask  $v_{i,j}$ :

$$V_{i,j} = (V_x)_{i,j} \cdot (V_y)_{i,j}, \quad (10)$$

where

$$\begin{aligned} (V_x)_{i,j} &= \begin{cases} 1 & (\partial_x, z)_{i,j} < z_{i,j} \cdot \beta \\ 0 & \text{otherwise} \end{cases} \\ (V_y)_{i,j} &= \begin{cases} 1 & (\partial_y, z)_{i,j} < z_{i,j} \cdot \beta \\ 0 & \text{otherwise} \end{cases} \end{aligned} \quad (11)$$

The validity mask  $V_{i,j}$  is used to zero out the spatial gradients at depth discontinuities:

$$\begin{aligned} (\partial x, \vec{r}')_{i,j} &= (\partial x, \vec{r})_{i,j} \cdot V_{i,j} \\ (\partial y, \vec{r}')_{i,j} &= (\partial y, \vec{r})_{i,j} \cdot V_{i,j} \end{aligned} \quad (12)$$

We then compute the average spatial derivatives over a window of size  $N \times N$  pixels around each pixel  $(i, j)$ :

$$\begin{aligned} \overline{(\partial x, \vec{r})}_{i,j} &= \frac{1}{N^2} \sum_{i',j'}^N (\partial x, \vec{r}')_{i-\frac{N}{2}+i', j-\frac{N}{2}+j'} \\ \overline{(\partial y, \vec{r})}_{i,j} &= \frac{1}{N^2} \sum_{i',j'}^N (\partial y, \vec{r}')_{i-\frac{N}{2}+i', j-\frac{N}{2}+j'} \end{aligned} \quad (13)$$

Note that we normalize by  $N^2$ , whereas the proper normalization would be by  $\sum_{i',j'} V_{i-\frac{N}{2}+i', j-\frac{N}{2}+j'}$ . However since the direction of the surface normal is insensitive to the norms of  $(\partial x, \vec{r})_{i,j}$  and  $(\partial y, \vec{r})_{i,j}$ , as opposed to their directions, this is immaterial.

To obtain the surface normal, we calculate the cross product of  $(\partial x, \vec{r})_{i,j}$  and  $(\partial y, \vec{r})_{i,j}$ ,

$$(\vec{n}_d)_{i,j} = \overline{(\partial x, \vec{r})}_{i,j} \times \overline{(\partial y, \vec{r})}_{i,j} \quad (14)$$

and then normalize it, to obtain the normalized surface normal:

$$(\hat{n}_d)_{i,j} = (\vec{n}_d)_{i,j} / \|(\vec{n}_d)_{i,j}\| \quad (15)$$

The consistency is then computed as

$$\mathcal{L}_{\text{con\_normals}} = \text{cosine\_distance}(\hat{n}_d, \hat{n}_p), \quad (16)$$

where  $\hat{n}_d$  is the computed surface normals from the inferred depth as described in this section, and  $\hat{n}_p$  is the normal map predicted from the normal prediction network.